Spectroscopy and Thermometry of Drumhead Modes in a Mesoscopic Trapped-Ion Crystal Using Entanglement

Brian C. Sawyer,[1,*] Joseph W. Britton,[1] Adam C. Keith,[2,†] C.-C. Joseph Wang,[2] James K. Freericks,[2] Hermann Uys,[3] Michael J. Biercuk,[4] and John J. Bollinger[1]

[1]*Time and Frequency Division, National Institute of Standards and Technology, Boulder, Colorado 80305, USA*
[2]*Department of Physics, Georgetown University, Washington, D.C. 20057, USA*
[3]*Council for Scientific and Industrial Research, Pretoria, South Africa*
[4]*Centre for Engineering Quantum Systems, School of Physics, The University of Sydney, NSW Australia*
(Received 30 January 2012; published 24 May 2012)

We demonstrate spectroscopy and thermometry of individual motional modes in a mesoscopic 2D ion array using entanglement-induced decoherence as a method of transduction. Our system is a $\sim$400 μm-diameter planar crystal of several hundred $^9Be^+$ ions exhibiting complex drumhead modes in the confining potential of a Penning trap. Exploiting precise control over the $^9Be^+$ valence electron spins, we apply a homogeneous spin-dependent optical dipole force to excite arbitrary transverse modes with an effective wavelength approaching the interparticle spacing ($\sim$ 20 μm). Center-of-mass displacements below 1 nm are detected via the entanglement of spin and motional degrees of freedom.

Studies of quantum physics at the interface of microscopic and mesoscopic regimes have recently focused on the observation of quantum coherent phenomena in optomechanical systems [1–3]. The realization of quantum coherence in mechanical oscillations involving many particles behaving approximately as a continuum provides exciting insights into the quantum-classical transition. Previous work has shown that crystals of cold, trapped ions behave as atomic-scale nanomechanical oscillators [4–6], with the benefits of *in situ* tunable motional modes and exploitable single-particle quantum degrees of freedom (e.g., valence electron spin). Our system of hundreds of crystallized ions in a Penning trap provides a bottom-up approach to studying mesoscopic quantum coherence. In this context, the relevant particle numbers are sufficiently small to permit excellent quantum control without sacrificing continuum mechanical features. Beyond these capabilities, trapped ions have long provided a laboratory platform for studying diverse physical phenomena including strongly coupled one-component plasmas [7,8], quantum computation [9,10] and simulation [11–15], dynamical decoupling [16], and atomic clocks and precision measurement [17].

In this Letter, we present an experimental and theoretical study of motional drumhead modes in a 2D crystal of $^9Be^+$ ions confined within a Penning trap. We excite *inhomogeneous* modes of arbitrary wavelength [see Fig. 1(a)] through the application of a *homogeneous*, spin-state-dependent optical dipole force (ODF) to a large-scale spin superposition. Distinct drumhead modes are entangled with the $^9Be^+$ valence electron spins by tuning a beat frequency (μ_R) between two ODF lasers near a mode resonance. This spin-motion entanglement is detected as a μ_R-dependent decoherence of ion spins whose magnitude conveys the specific mode temperature.

Previous global mode studies on 2D planar ion arrays were restricted to modes with wavelengths on the order of the cloud size [18–22]. By contrast, the short-wavelength modes studied here are of particular interest due to their increased sensitivity to strong-correlation corrections [23,24] compared to those with a long wavelength, which are well described by fluid theory. Thermometry of large Coulomb crystals has thus far been limited to mode-insensitive Doppler profile measurements [25], which give a minimum detectable temperature of $\sim$0.5 mK in $^9Be^+$. Our temperature measurement is mode specific and may be employed below the Doppler cooling limit, providing an alternative to Raman sideband thermometry [26].

The Penning trap used for this work is detailed in a previous publication [27]. The application of static voltages to a stack of cylindrical electrodes provides harmonic confinement along $\hat{z}$ (the trap symmetry axis) with a $^9Be^+$ center-of-mass (c.m.) oscillation frequency of $\omega_1/2\pi =$ 795 kHz that is independent of the number of trapped ions. The trap resides within the room-temperature bore of a superconducting magnet, and radial confinement is achieved via the Lorentz force generated by rotation of the ion cloud through the static, homogeneous magnetic (B) field of $\sim$4.46 T oriented along $\hat{z}$. Application of a time-dependent quadrupole "rotating wall" potential permits phase-stable control of the rotation frequency (ω_r) and thus, the confining radial force of the trap [28,29]. In the limit of a weak rotating wall potential, the harmonic trap potential in a frame rotating at ω_r is [8]

$$q\Phi_{\mathrm{trap}}(r, z) = \tfrac{1}{2}M\omega_1^2(z^2 + \beta r^2), \qquad (1)$$

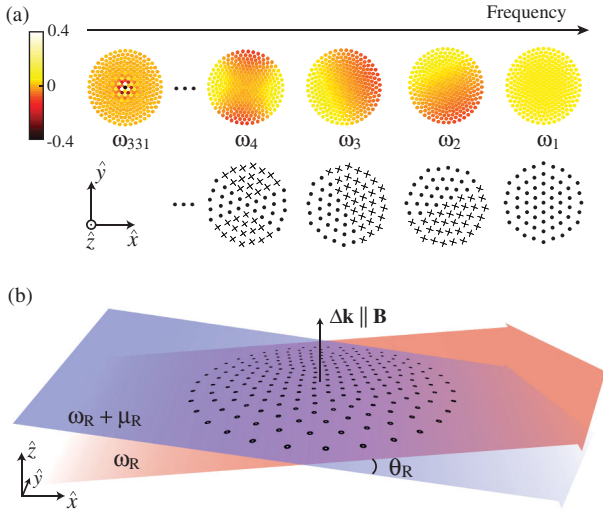$$\beta = \frac{\omega_r(\Omega_c - \omega_r)}{\omega_1^2} - \frac{1}{2}, \qquad (2)$$

FIG. 1 (color). (a) Calculated structure of selected transverse eigenmodes ($\vec{b}_m$) for a 2D crystal of 331 $^9Be^+$ ions. Mode frequencies, ω_m, decrease as the effective wavelength gets shorter. The arbitrary color scale indicates relative ion displacement amplitude. One example of an ion spin state with similar symmetry is given below each of the four highest-frequency eigenmodes. The symbol $\times(\bullet)$ denotes spin-projection into (out of) the plane. Interaction between these spin and mode configurations mediated by the spin-dependent ODF leads to excitation of the corresponding eigenmode. (b) Illustration of a single plane of $^9Be^+$ within the Penning trap. Two 313-nm beams intersect at the ion crystal to form a traveling wave of beat frequency μ_R and effective wave vector $\vec{\Delta k}$ along the direction of the trap magnetic field. The electric field intensity is uniform in the plane, but the spin-dependent induced ac Stark shift permits excitation of transverse modes of arbitrary wavelength using the pulse sequence of Fig. 2(a).

where M (q) is the mass (charge) of a single $^9Be^+$, $\Omega_c = 2\pi \times 7.6$ MHz is the cyclotron frequency, and z (r) is the axial (radial) distance from the trap center. We set the rotation frequency, ω_r, such that the radial confinement is weak relative to transverse confinement ($\beta \ll 1$), resulting in a single ion plane.

The $m_J = \pm 1/2$ projections of the Be^+ $^2S_{1/2}$ ground state are split by ~ 124 GHz and serve as $|\uparrow\rangle$ and $|\downarrow\rangle$ "qubit" states, respectively. Global spin rotations are performed by injecting 124-GHz radiation through a waveguide attached to the side of the trap. The $^9Be^+$ ions are Doppler laser cooled with laser beams directed both parallel and perpendicular to $\hat{z}$. Both beams are tuned ~ 5 MHz below the $^2S_{1/2}(m_J = +1/2) - ^2P_{3/2}(m_J = +3/2)$ transition at ~ 313 nm whose Doppler cooling limit is 0.43 mK. This same transition is used for ion detection and projective spin-state measurement. Discrimination of $|\uparrow\rangle$ (bright) from $|\downarrow\rangle$ (dark) is performed with a fidelity >99% [27].

The axial and radial confining potentials are tuned to yield a single plane of ions. Because of mutual Coulomb

repulsion and the low ion temperature, the ions' minimum-energy configuration is a 2D crystal with a triangular order [30]. Ion spacing is ~ 20 μm, and individual ions can be resolved using stroboscopic imaging at ω_r. The planar array of N ions exhibits $3N$ motional modes, N of which are drumhead oscillations transverse to the crystal plane [see Fig. 1(a)]. As with 1D ion strings, the frequencies of these transverse modes decrease with decreasing effective wavelength due to the screening of confining electric fields by nearby ions. The transverse eigenvectors ($\vec{b}_m$, $m \in [1, N]$) and corresponding eigenfrequencies (ω_m) are obtained by first numerically calculating the zero-temperature 2D ion configuration in the presence of the Penning trap potentials. Applying a Taylor expansion of the combined trap and Coulomb potential about each ion equilibrium position, we diagonalize the $N \times N$ stiffness matrix whose eigenvalues and unit eigenvectors are ω_m and $\vec{b}_m$, respectively [14,31,32]. The relative displacement amplitude of an ion j is given by the jth element of $\vec{b}_m$, denoted as b_{jm}, where $\sum_m |b_{jm}|^2 = \sum_j |b_{jm}|^2 = 1$.

To excite transverse modes in our 2D Coulomb crystal, we employ a spin-dependent ODF generated by interfering two off-resonant laser beams at the ion crystal position. This is depicted schematically in Fig. 1(b). The two ODF beams are produced from a single beam using a 50/50 beam splitter and subsequently pass through separate acousto-optic modulators that allow fast (~ 1 μs) switching and impart a relative detuning μ_R. The beams intersect at an angle of $\theta_R = 4.8° \pm 0.2°$ at the ion cloud position, and their relative alignment is adjusted to orient the effective wave vector ($\vec{\Delta k}$) of the resulting standing ($\mu_R = 0$) or traveling ($\mu_R \neq 0$) wave to within $\sim 0.05°$ of $\hat{z}$. The wavelength (313.133 nm) and polarizations of the beams are chosen such that the ac Stark shift from the interfering beams on state $|\uparrow\rangle$ is equal in magnitude and opposite in sign to that on $|\downarrow\rangle$ [33]. The result of the interference between these two beams is a spin-dependent force on each ion, j ($F_{\uparrow,j} = -F_{\downarrow,j} \equiv F_j$). The Hamiltonian for this interaction is $\hat{H}_{ODF} = -\sum_{j=1}^{N} F_j \hat{z}_j(t) \cos(\mu_R t) \hat{\sigma}_j^z$, where $\hat{z}_j(t)$ is the time-dependent position operator and $\hat{\sigma}_j^z$ is the z-component Pauli operator for ion j [14]. The elliptical beam waists (100 μm $\times$ 1000 μm, with the major axis oriented parallel to the ion plane [33]) are sufficiently large to generate an approximately uniform ODF with variation below 10% across the ~ 400 μm-diameter planar ion crystal. Typical ODFs for this work are $F_j \sim 10^{-23}$ N along $\hat{z}$.

Figure 2(a) illustrates the experimental control sequence for microwaves (black line) and ODF lasers (shaded regions) used to coherently excite transverse modes of motion. Ions are first prepared in the "bright" state $|\uparrow\rangle_N \equiv \bigotimes_{j=1}^{N} |\uparrow_j\rangle$ via optical pumping [27]. The sequence of microwave pulses in Fig. 2(a) comprises a spin echo (SE) [34] that, in the absence of the ODF beams, rotates the ions to the "dark" state $|\downarrow\rangle_N$ with >99% fidelity. The SE cancels
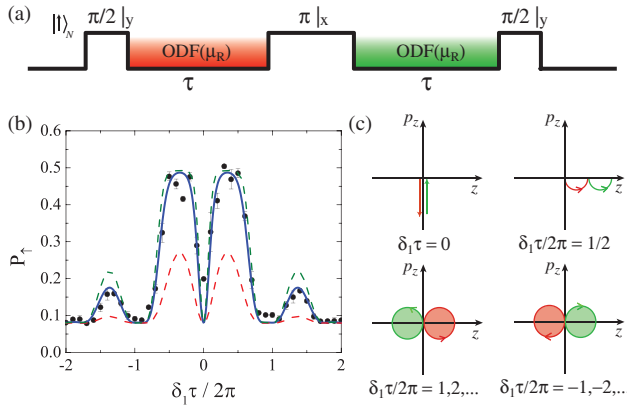
FIG. 2 (color). (a) Pulse sequence used for excitation and detection of transverse motional modes. Global spin rotations are performed with microwaves at ~124 GHz, while the state-dependent optical dipole force is applied in each arm of the spin echo for a duration τ. We implement π-pulse times (t_π) as short as 65 μs. (b) Measured (points with statistical error bars) and fit (solid blue line) probability of detecting $|\uparrow\rangle$ ($P_\uparrow$) at the end of the spin echo sequence. Frequency-dependent decoherence is due to the entanglement of spins with the axial c.m. mode ($\omega_1/2\pi =$ 795 kHz) as a function of ODF detuning $\delta_1 \equiv \mu_R - \omega_1$ in a cloud of 190 ± 8 ions. Each point is an average of 90 experimental runs. The fit provides a mode temperature of 2.3 ± 0.5 mK, whose error includes a 5% uncertainty in the ODF beam angle, θ_R. For comparison, the lower (upper) dashed line is calculated assuming 0.4 mK (4.0 mK). (c) Illustrated phase-space trajectories of state $|\uparrow\rangle_N$ at different detunings, δ_1, in a frame rotating at ω_1. Axis labels represent c.m. momentum ($p_z \propto \text{Im}[\alpha_{j1}]$) and position ($z \propto \text{Re}[\alpha_{j1}]$).

low-frequency precession about $\hat{z}$ due to ODF laser intensity and magnetic field fluctuations as well as microwave phase noise [16,35]. The spin-dependent ODF is applied in each arm of the SE for a duration τ.

The initial microwave pulse rotates each spin by $\pi/2$ to produce the state $\bigotimes_{j=1}^{N} \frac{1}{\sqrt{2}}(|\uparrow_j\rangle - |\downarrow_j\rangle)$, which is a superposition of all possible (2^N) spin permutations. Importantly, it is the creation of this state that permits subsequent excitation of arbitrary transverse modes with our homogeneous, spin-dependent ODF. By tuning μ_R near a mode of frequency ω_m, the spin-dependent ODF excites those components of the spin superposition with approximately the same symmetry as the eigenvector $\vec{b}_m$. A subset of these eigenvectors and associated spin states are illustrated in Fig. 1(a). Depending on experimental parameters, the spin states may be entangled with different motional states at the end of the control sequence of Fig. 2(a). Upon measurement of the spin state (performing a trace over the motion), entanglement is manifested as spin decoherence that varies with μ_R. We observe this as a decrease in the length of the spins' Bloch vector and a concomitant increase in the probability ($P_\uparrow$) of measuring state $|\uparrow\rangle$ averaged over all ions.

Figure 2(b) gives experimental and theoretical results for a sweep of μ_R near the c.m. frequency, ω_1, with

$\tau = 500$ μs and $\delta_1 = (\mu_R - \omega_1)$. On resonance ($\delta_1 = 0$), the pulse sequence leads to excitation (deexcitation) of the c.m. mode in the first (second) arm. When the product $|\delta_1\tau/2\pi| = l$ is a nonzero integer, each spin state traverses l full loops in phase space over τ [see Fig. 2(c)]. At intermediate detunings, the spin and motion remain entangled at the end of the pulse sequence, producing the line shape of Fig. 2(b). These motional excitations are described by the spin-dependent displacement operator $\hat{U}(\tau) = \prod_{j,m} \exp[(\alpha_{jm}\hat{a}_m^\dagger - \alpha_{jm}^*\hat{a}_m)\hat{\sigma}_j^z]$ [32,33,36], where $\alpha_{jm}(\tau)$ is the coherently driven complex displacement amplitude for ion j of mode m, and $\hat{a}_m^\dagger(\hat{a}_m)$ is the creation (annihilation) operator for mode m. Accounting for both arms of the pulse sequence, we obtain [33]

$$\alpha_{jm} = \frac{F_j b_{jm}}{\hbar(\mu_R^2 - \omega_m^2)} \sqrt{\frac{\hbar}{2M\omega_m}} (\omega_m(1 - \cos\phi) + i\mu_R \sin\phi$$
$$- e^{i\omega_m\tau}\{\omega_m[\cos(\mu_R\tau) - \cos(\mu_R\tau + \phi)]$$
$$- i\mu_R[\sin(\mu_R\tau) - \sin(\mu_R\tau + \phi)]\}), \quad (3)$$

where $\hbar$ is Planck's constant, F_j is the ODF magnitude on ion j, and $\phi = (\tau + t_\pi)(\mu_R - \omega_m)$ accounts for phase evolution of the ODF drive relative to that of the mode.

Although the coherently driven, spin-dependent displacements (α_{jm}) are independent of the initial motional state (assuming Lamb-Dicke confinement [14]), the spin-motion entanglement signal in Fig. 2(b) sensitively depends on this initial state. This can be qualitatively understood in terms of the spatial structure of a harmonic oscillator Fock state, $|n_m\rangle$, of mode m. The wave function of state $|n_m\rangle$ exhibits n nodes and therefore, as n increases, a fixed spin-dependent displacement results in less wave function overlap between different spin components due to the increasing spatial frequency of $|n_m\rangle$ wave functions. This leads to larger decoherence and greater displacement sensitivity as the average mode occupation, $\bar{n}_m$, is increased for a given mode. We fit the experimental measurements in Fig. 2(b) using theory that attributes a thermal state of motion to each mode m characterized by the mode occupation $\bar{n}_m \sim k_B T_m (\hbar\omega_m)^{-1}$ and temperature T_m. Neglecting spin-spin correlation contributions, we find the probability $P_\uparrow^{(j)}$ of detecting ion j in state $|\uparrow\rangle$ at the end of the pulse sequence to be [33]

$$P_\uparrow^{(j)} = \frac{1}{2}\left[1 - e^{-2\Gamma\tau} \exp\left(-2\sum_m |\alpha_{jm}|^2 (2\bar{n}_m + 1)\right)\right]. \quad (4)$$

Here Γ accounts for decoherence due to spontaneous emission induced by the ODF lasers over the duration 2τ, and is responsible for the background level of $P_\uparrow \sim 0.1$ observed in all experimental data presented here [37]. The total detection probability $P_\uparrow$ is obtained by averaging all $P_\uparrow^{(j)}$.

For interaction with the c.m. mode ($b_{j1} = \frac{1}{\sqrt{N}}$, $\forall\, j \in$ [1, N]), α_{j1} is obtained from Eq. (3) through measurement of the ODF laser intensities [14] and trapped-ion number, while Γ is determined from decoherence observed with μ_R detuned far from any modes. As such, the only parameter of Eq. (4) not measured directly is $\bar{n}_1$, which is varied to fit experimental data as in Fig. 2(b), where we obtain $\bar{n}_1 = 60 \pm 13$ ($T_1 = 2.3 \pm 0.5$ mK).

We note that a detectable decoherence signal is obtained with a very small amplitude of $|\alpha_{jm}|$. For example, in Fig. 2(b), the 20% decrease in the Bloch vector at $\delta_1\tau/2\pi \simeq \pm 1.4$ corresponds to a spin-state-dependent excitation of the c.m. mode with a mean excursion of ~ 0.6 nm in each arm of the pulse sequence. This shift is less than 0.2% of the wave function spread of a single ion in the planar array. Our sensitivity to displacements improves with increasing mode temperature provided that the ODF is adjusted to avoid full decoherence ($P_\uparrow = 0.5$) at the detuning of interest.

Figure 3(a) shows the result of a sweep of μ_R over five transverse modes and corresponding theory. The theoretical spectrum (offset for clarity) is generated assuming $T_1 = 10$ mK and $T_{m>1} = 0.4$ mK, with T_1 obtained from a fit. The large c.m. temperature of Fig. 3(a) is produced by quickly switching off the $\hat{z}$-oriented Doppler cooling beam on a time scale of $\sim 2\pi\omega_1^{-1}$. In this case, a sudden loss of radiation pressure from the cooling light induces a c.m. oscillation amplitude of ~ 50 nm that we detect as an elevated $\bar{n}_1$. A more adiabatic reduction of the cooling beam intensity yields $\bar{n}_1 \sim 26$ ($T_1 \sim 1$ mK). For modes other than the c.m., we must additionally calculate the b_{jm} values for the trap potentials and ion number in a given

experiment [14]. For these modes, we find temperatures consistent with the Doppler cooling limit of 0.43 mK.

To measure the full spectrum of transverse modes, we repeat the sequence of Fig. 2(a) for 30 kHz $\leq \mu_R/2\pi \leq$ 800 kHz with $\tau = 1$ ms. With the exception of the c.m. mode, the frequencies of the remaining $N - 1$ modes depend sensitively on our choice of crystal rotation frequency, ω_r [20]. Figures 3(b) and 3(c) show the result of these experimental runs for $\omega_r/2\pi = 43.2$ and 44.7 kHz, respectively. For this ion number of 345 ± 25, the single-plane configuration is stable over the range 42.2 kHz $\lesssim \omega_r/2\pi \lesssim 45.2$ kHz. Histograms of calculated mode density versus $\mu_R/2\pi$ are plotted below each experimental curve with an arbitrary vertical scale and bin width of 10 kHz. The distribution of eigenfrequencies narrows as ω_r is decreased; weaker radial confinement [see Eq. (2)] leads to lower ion densities and a reduced screening of trap potentials, thereby moving the frequency of the shortest-wavelength mode toward that of the c.m. This behavior is clearly visible in Figs. 3(b) and 3(c). Additionally, we find quantitative agreement between the measured spectrum and the mode density generated from numerical calculation of the transverse eigenmodes under the given experimental conditions, documenting coupling to both short- and long-wavelength modes. We believe the sharp features of Figs. 3(b) and 3(c) shaded in light green reflect excitation of in-plane resonances at harmonics of ω_r due to a very small component of the ODF ($\sim 10^{-3}F_j$) along the ion plane. These spectral features are reduced by more careful alignment of $\vec{\Delta k}$ to $\hat{z}$, but their strong response suggests an elevated motional temperature perpendicular to $\hat{z}$.
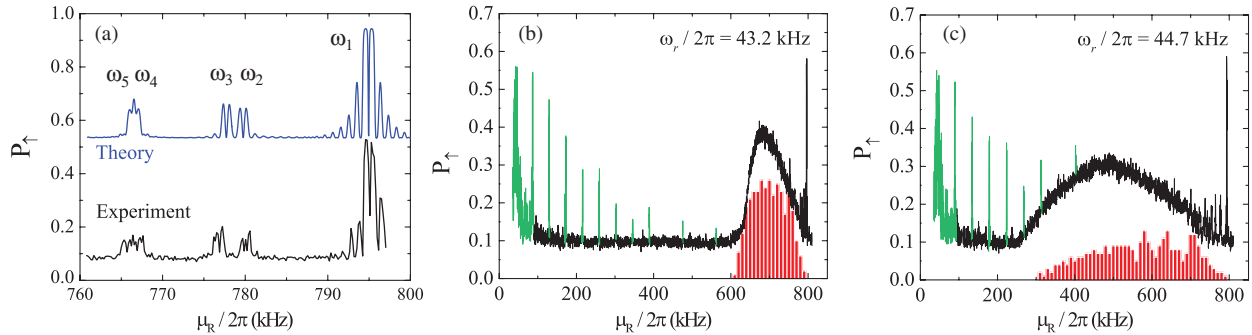

FIG. 3 (color).   (a) Measured (lower) and calculated (offset) probabilities for measuring $|\uparrow\rangle$ after the spin echo sequence as a function of ODF beat frequency for a sweep of μ_R over the first five transverse modes with 250 ± 15 ions. The modes at ω_2 and ω_3 are split due to the distortion of the ion cloud boundary by the rotating wall potential. Panels (b) and (c) give results of wider sweeps with $\omega_r/2\pi = 43.2$ and 44.7 kHz, respectively, in a crystal of 345 ± 25 ions. Frequency-dependent deviation from $P_\uparrow \sim 0.1$ is due to spin-motional entanglement, while the background is due to spontaneous emission from the ODF beams. The histogram (red bars) shown below each experimental curve depicts the density of calculated eigenmodes at the given ω_r. Histogram bins are 10 kHz wide and plotted with an arbitrary vertical scale. As described in Fig. 1(a), the highest-frequency feature is that of the c.m. mode and the ~ 50 lowest-frequency eigenmodes include nearest-neighbor ions oscillating out of phase. Features at ω_r and precise harmonics thereof (shaded in light green) are believed to be due to spin-motion entanglement with in-plane degrees of freedom excited by the small ($\sim 10^{-3}F_j$) component of ODF perpendicular to $\hat{z}$.

In summary, we have used the entanglement of spin and motional degrees of freedom to map the full transverse mode spectrum of a mesoscopic 2D ion array. This technique provides a tool for sensitively and accurately measuring the temperature and displacement amplitude of individual drumhead modes, facilitating the identification of mode-specific heating mechanisms and the resulting nonequilibrium energy distributions. Coherent, spin-dependent excitation of transverse modes is the basis for engineering quantum spin-spin interactions with trapped ions [11–14,31,32,38,39], making mode characterization a critical element of such experiments. Future work will include the investigation of low-frequency in-plane modes at frequencies smaller than ω_r. A predicted subset of these modes includes in-plane shearing motion whose restoring force is due exclusively to strong correlations.

---

*brian.sawyer@boulder.nist.gov

†Present address: Department of Physics, North Carolina State University, Raleigh, NC 27695, USA.

[1] A. D. O'Connell et al., Nature (London) **464**, 697 (2010).

[2] T. J. Kippenberg and K. J. Vahala, Science **321**, 1172 (2008).

[3] J. D. Teufel, T. Donner, M. A. Castellanos-Beltran, J. W. Harlow, and K. W. Lehnert, Nature Nanotech. **4**, 820 (2009).

[4] M. J. Biercuk, J. W. Britton, H. Uys, A. VanDevender, and J. J. Bollinger, Nature Nanotech. **5**, 646 (2010).

[5] J. D. Jost, J. P. Home, J. M. Amini, D. Hanneke, R. Ozeri, C. Langer, J. J. Bollinger, D. Leibfried, and D. J. Wineland, Nature (London) **459**, 683 (2009).

[6] K. R. Brown, C. Ospelkaus, Y. Colombe, A. C. Wilson, and D. J. Wineland, Nature (London) **471**, 196 (2011).

[7] S. Ichimaru, Rev. Mod. Phys. **54**, 1017 (1982).

[8] D. H. E. Dubin and T. M. O'Neil, Rev. Mod. Phys. **71**, 87 (1999).

[9] D. Hanneke, J. P. Home, J. M. Amini, D. Leibfried, and D. J. Wineland, Nature Phys. **6**, 13 (2009).

[10] T. Monz et al., Phys. Rev. Lett. **103**, 200503 (2009).

[11] A. Friedenauer, H. Schmitz, J. T. Glueckert, D. Porras, and T. Schaetz, Nature Phys. **4**, 757 (2008).

[12] K. Kim, M.-S. Chang, S. Korenblit, R. Islam, E. E. Edwards, J. K. Freericks, G.-D. Lin, L.-M. Duan, and C. Monroe, Nature (London) **465**, 590 (2010).

[13] R. Islam et al., Nature Commun. **2**, 377 (2011).

[14] J. W. Britton, B. C. Sawyer, A. C. Keith, C.-C. J. Wang, J. K. Freericks, H. Uys, M. J. Biercuk, and J. J. Bollinger, Nature (London) **484**, 489 (2012).

[15] B. P. Lanyon et al., Science **334**, 57 (2011).

[16] M. J. Biercuk, H. Uys, A. P. VanDevender, N. Shiga, W. M. Itano, and J. J. Bollinger, Nature (London) **458**, 996 (2009).

[17] T. Rosenband et al., Science **319**, 1808 (2008).

[18] D. J. Heinzen, J. J. Bollinger, F. L. Moore, W. M. Itano, and D. J. Wineland, Phys. Rev. Lett. **66**, 2080 (1991).

[19] J. J. Bollinger, D. J. Heinzen, F. L. Moore, W. M. Itano, D. J. Wineland, and D. H. E. Dubin, Phys. Rev. A **48**, 525 (1993).

[20] C. S. Weimer, J. J. Bollinger, F. L. Moore, and D. J. Wineland, Phys. Rev. A **49**, 3842 (1994).

[21] M. D. Tinkle, R. G. Greaves, C. M. Surko, R. L. Spencer, and G. W. Mason, Phys. Rev. Lett. **72**, 352 (1994).

[22] A. Dantan, J. P. Marler, M. Albert, D. Guénot, and M. Drewsen, Phys. Rev. Lett. **105**, 103001 (2010).

[23] J. M. Kriesel, J. J. Bollinger, T. B. Mitchell, L. B. King, and D. H. E. Dubin, Phys. Rev. Lett. **88**, 125003 (2002).

[24] J. Castro, P. McQuillen, and T. C. Killian, Phys. Rev. Lett. **105**, 065004 (2010).

[25] M. J. Jensen, T. Hasegawa, and J. J. Bollinger, Phys. Rev. A **70**, 033401 (2004).

[26] C. Monroe, C. Monroe, D. M. Meekhof, B. E. King, S. R. Jefferts, W. M. Itano, D. J. Wineland, and P. Gould, Phys. Rev. Lett. **75**, 4011 (1995).

[27] M. J. Biercuk, H. Uys, A. P. VanDevender, N. Shiga, W. M. Itano, and J. J. Bollinger, Quantum Inf. Comput. **9**, 920 (2009).

[28] T. Hasegawa, M. J. Jensen, and J. J. Bollinger, Phys. Rev. A **71**, 023406 (2005).

[29] X.-P. Huang, J. J. Bollinger, T. B. Mitchell, W. M. Itano, and D. H. E. Dubin, Phys. Plasmas **5**, 1656 (1998).

[30] T. B. Mitchell, J. J. Bollinger, D. H. E. Dubin, X.-P. Huang, W. M. Itano, and R. H. Baughman, Science **282**, 1290 (1998).

[31] S.-L. Zhu, C. Monroe, and L.-M. Duan, Phys. Rev. Lett. **97**, 050505 (2006).

[32] K. Kim, M.-S. Chang, R. Islam, S. Korenblit, L.-M. Duan, and C. Monroe, Phys. Rev. Lett. **103**, 120502 (2009).

[33] See Supplemental Material at http://link.aps.org/supplemental/10.1103/PhysRevLett.108.213003 for technical details and derivations.

[34] E. L. Hahn, Phys. Rev. **80**, 580 (1950).

[35] H. Uys, M. J. Biercuk, and J. J. Bollinger, Phys. Rev. Lett. **103**, 040501 (2009).

[36] C. Monroe, D. M. Meekhoff, B. E. King, and D. J. Wineland, Science **272**, 1131 (1996).

[37] H. Uys, M. J. Biercuk, A. P. VanDevender, C. Ospelkaus, D. Meiser, R. Ozeri, and J. J. Bollinger, Phys. Rev. Lett. **105**, 200401 (2010).

[38] D. Porras and J. I. Cirac, Phys. Rev. Lett. **92**, 207901 (2004).

[39] D. Porras and J. I. Cirac, Phys. Rev. Lett. **96**, 250501 (2006).